ChemComm

COMMUNICATION

View Article Online
View Journal

Cite this: DOI: 10.1039/d5cc06225j

Received 3rd November 2025,
Accepted 12th January 2026

DOI: 10.1039/d5cc06225j

rsc.li/chemcomm

Ruthenium or osmium? On the role of the metal in carbonylchlorido complexes for photodynamic therapy

Gina Elena Giacomazzo,[a] Fortuna Ponte,[b] Valentina Ceccherini,[a] Lorenzo Gianassi,[a] Gloria Mulas,[c] Emilia Sicilia,[b] Francesca Cencetti,[c] Barbara Valtancoli,[a] Luca Conti *[a] and Claudia Giorgi *[a]

Two novel carbonylchlorido complexes for photodynamic therapy (PDT), RuCOCl and OsCOCl, were synthesized *via* a unified synthetic strategy. Comparative photophysical, computational and preliminary biological studies reveal the crucial influence of the metal in governing their PDT performance, highlighting the potential of this largely underestimated class of complexes for PDT applications.

Ruthenium(II) polypyridyl complexes (RPCs) have long stood as the photosensitizers (PSs) of choice as inorganic compounds for photodynamic therapy (PDT),[1–5] mainly thanks to the rich chemical-physical repertoire, encompassing tunable photophysical properties, efficient singlet oxygen ($^1O_2$) generation and interaction with key biological targets.[6,7] However, in recent years osmium(II)-based complexes have emerged as a promising alternative,[8–11] offering superior properties in terms of red-shifted absorptions,[10,12] spin–orbit coupling and chemical stability.[11,13] Yet, despite these advantages, their actual potential over Ru(II) analogues still remains largely unexplored, owing to the limited number of direct comparative investigations on the role of the metal in translating these features into tangible benefits for PDT.

Prompted by this scenario, herein we present a comparative study of two novel Ru(II) and Os(II) carbonylchlorido complexes, namely **RuCOCl** and **OsCOCl**, featuring the polypyridyl ligands 4,4′-dimethyl-2,2′-bipyridine (Me_2bpy) and benzo[i]dipyrido[3,2-a:2′,3′-c]phenazine (dppn) (Scheme 1). Although carbonylchlorido complexes are well known for different applications, spanning from carbon dioxide reduction[14–16] to hydrogen production,[17,18] their use in PDT remains, to the best of our knowledge, unexplored, leaving an important gap to be fulfilled. Incorporation of the dppn ligand in the two complexes is intended to enhance their PDT potential by enabling long-lived ^{3}IL ($^3\pi\pi^*$) states for $^1O_2$ sensitization, red-shifting the absorption and facilitating membrane permeation.[19–21] From a synthetic point of view, among the various strategies for the preparation of heteroleptic Ru(II) carbonylchlorido complexes $[Ru(NN)(N'N')COCl]^+$ (NN and N′N′ = different polypyridyl chelates), one of the most straightforward was described by Spiccia *et al.*,[22] involving a key photodecarbonylation step of a dicarbonyl $[Ru(NN)(CO)_2Cl_2]$ intermediate (Scheme S1, SI). However, this route is not straightforward for Os(II), owing to higher-energy d-d states and stronger CO backbonding that hinder photodecarbonylation.[23] Alternative methods replacing this step with chloride-triflate exchange have indeed been explored, although they lead to the dicarbonyl products rather than the desired carbonylchlorido analogues (Scheme S2, SI).[24] The different nature of the two metals, therefore, makes a unified synthetic method a non-trivial task yet essential to compare their reactivity. To this end, we developed a new strategy, applicable to both metals, for the preparation of analogous carbonylchlorido complexes (Scheme 1).

As shown, and described in detail in the SI (paragraph 1), the first step afforded the polymeric precursors $[Ru(CO)_2Cl_2]_n$ (**1a**) and $[Os(CO)_2Cl_2]_n$ (**1b**) by refluxing $RuCl_3{\cdot}3H_2O$ with formic acid and paraformaldehyde, in line with the literature for **1a**[22] and with slight modifications from Keene *et al.* for **1b**.[24] These showed similar reactivity in step II, coordinating Me_2bpy in alcoholic solvent to give $[Ru(Me_2bpy)(CO)_2Cl_2]$ (**2a**) and $[Os(Me_2bpy)(CO)_2Cl_2]$ (**2b**), both of them showing *cis*-dicarbonyl *trans*-dichloro configuration, according to the literature and in line with the C_{2v} molecular symmetries of NMR analysis (Fig. S1 and S2, SI).[22,24] **RuCOCl** and **OsCOCl** were then obtained by chemical decarbonylation of **2a** and **2b**, which were reacted with dppn in 2-methoxyethanol in the presence of trimethylamine *N*-oxide (TMAO) as a decarbonylating agent, leading to the final complexes as hexafluorophosphate salts, following KPF_6 precipitation (step III). The overall yield over three synthetic steps was 29% for **RuCOCl** and 18% for **OsCOCl**. Ru(II) and Os(II) complexes were obtained as nearly 1 : 1 mixtures of *trans*-CO and *trans*-Cl isomers, as shown by NMR data and

[a] *Department of Chemistry "Ugo Schiff", University of Florence, Via della Lastruccia 3, 50019, Sesto Fiorentino (FI), Italy. E-mail: luca.conti@unifi.it, claudia.giorgi@unifi.it*
[b] *Department of Chemistry and Chemical Technologies University of Calabria, via Pietro Bucci, 87036 Arcavacata Rende, Cs, Italy*
[c] *Department of Experimental and Clinical Biomedical Sciences "Mario Serio", University of Florence, Viale Morgagni 50, Florence 50134, Italy*

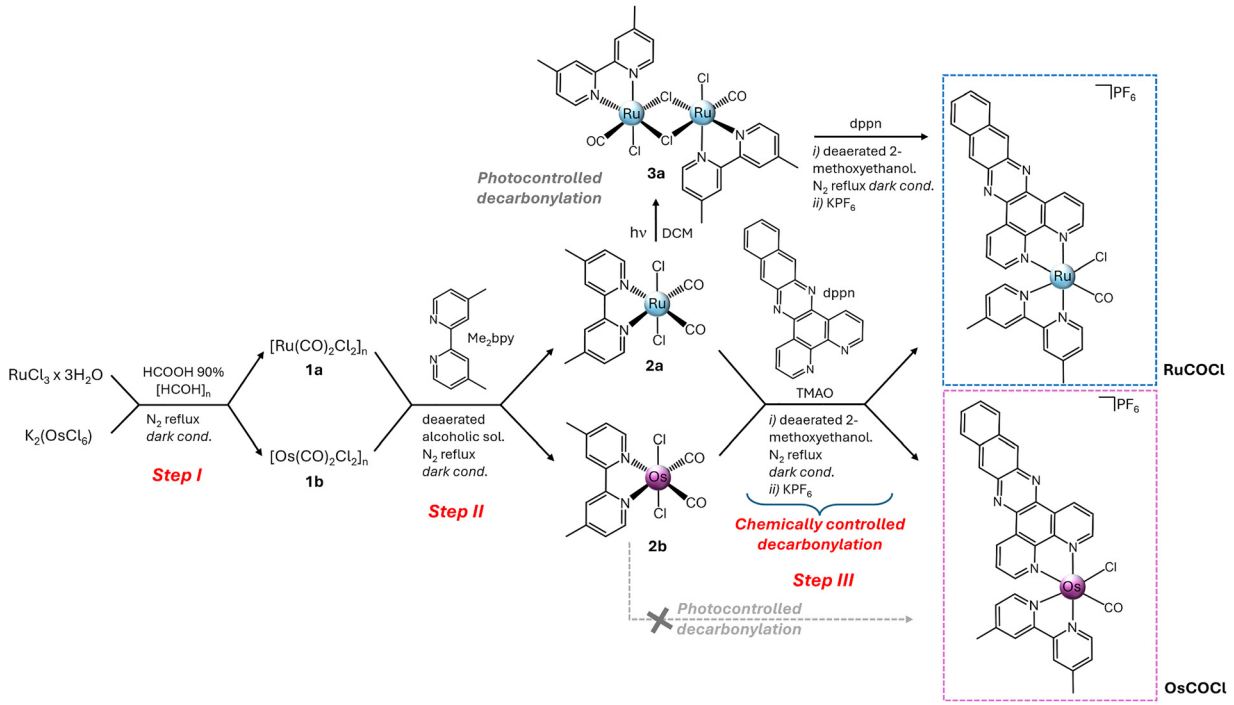

Scheme 1 Synthetic strategy for obtaining carbonylchlorido complexes **RuCOCl** and **OsCOCl**.

consistent with the literature (Fig. S3, S5, S6, S8, SI).[24,25] HR-(ESI) MS analysis further confirmed the identity of the compounds, as denoted by the isotopic patterns of the mono positively charged [**RuCOCl**-PF_6]$^+$ and [**OsCOCl**-PF_6]$^+$, centered at 681.07566 and 771.13319 (m/z = 1) (Fig. S4, S7, SI). Isomer separation was not achievable chromatographically; however, a *trans*-CO enriched mixture (67 : 33), referred to as **OsCOCl-67**, was obtained by exploiting their different solubilities in acetone and dichloromethane (Fig. S8, SI); this sample was also included in the chemical-physical analysis, shown in Fig. 1.

The introduction of a controlled chemical decarbonylation in step III was crucial to give **OsCOCl**, since **2b** does not undergo photodecarbonylation unlike its Ru(II) analogue, and therefore, to provide a common synthetic pathway for both the

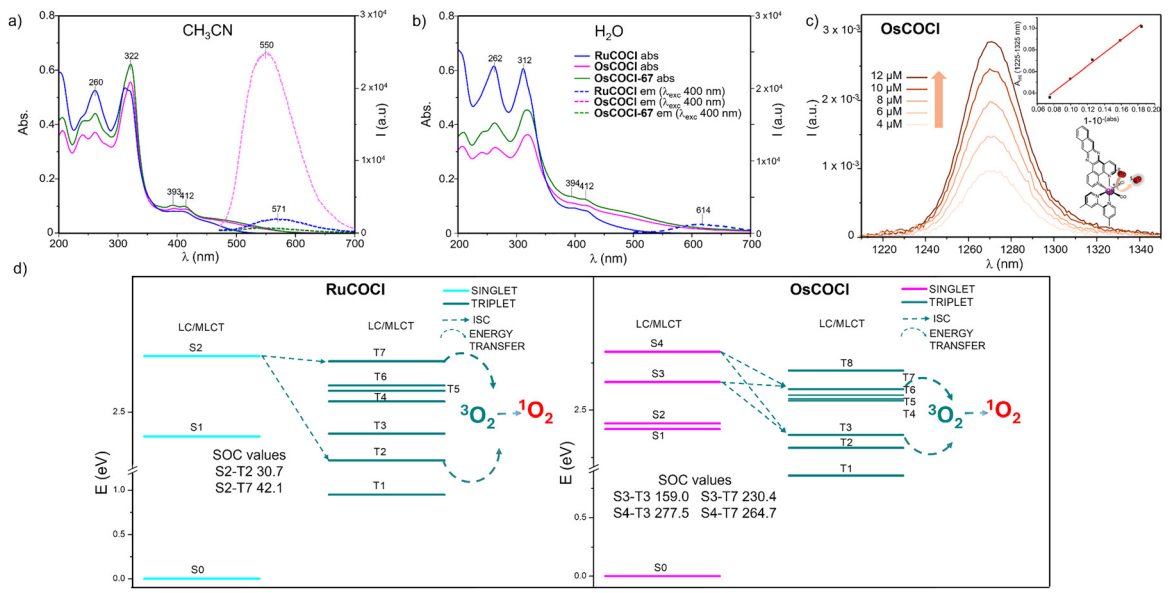

Fig. 1 Absorption and emission spectra of acetonitrile (a) and aqueous (b) solutions of **RuCOCl**, **OsCOCl** and **OsCOCl-67** (10 μM). (c) Singlet oxygen determination by direct measurement of the $^1O_2$ phosphorescence at 1270 nm in **OsCOCl** acetonitrile solutions. (d) Jablonski-like diagram representing the most probable ISC processes for the **RuCOCl** and **OsCOCl** complexes allowing the population of the triplet states. Only the largest spin–orbit coupling matrix elements are reported.

final complexes. The difference in reactivity of dicarbonyl intermediates, clearly imparted by the nature of the metal, was further investigated by density functional theory (DFT) and time-dependent density functional theory (TDDFT) calculations, performed on **2a** and **2b** in both the ground and excited state. All calculations, including geometry optimizations, relaxed scan analyses, UV-visible spectral simulations, and natural bond orbital (NBO) analysis, were performed at the B3PW91 level of theory and are described in detail in paragraph 5.1, SI. Our data showed that, when irradiated, the CO release from the Ru(II)-based **2a** occurs with a low activation barrier (2.1 kcal mol^{-1}) following an exergonic reaction, whereas for **2b** the energy barrier is higher (17 kcal mol^{-1}) and the process is endergonic. Thus, CO dissociation is both kinetically and thermodynamically favoured for the Ru(II) intermediate but disfavoured for its Os(II) analogue (Fig. S13, SI). This, along with the NBO analysis which revealed a weaker LP(Ru) → π(CO)* back-donation compared to Os(II), corroborated the observed higher inertness of the Os(II)-CO bond in **2b** and the consequent need for a more energetic decarbonylation reaction.

Absorption and emission spectra of the complexes in acetonitrile and water are shown in Fig. 1; their molar extinction coefficients (ε), fluorescence maxima (λ_{em}) and fluorescence emission quantum yields (φ_L) are listed in Table 1. Of particular relevance in the UV-vis spectra is the panchromatic ^{1}MLCT absorption of **OsCOCl**, with a tail extending beyond 550 nm, better matching the therapeutic window. This effect, which represents a key reason for the strong appeal of Os(II) complexes in PDT,[26,27] is even more evident in water (Fig. 1b). Fluorescence emissions are overall moderate, consistent with the population of low-lying triplet states of mixed ligand centered/MLCT character (Fig. 1d), with a significant contribution from poorly emissive, dppn-centered ^{3}LC ($^3\pi\pi^*$) states (see also paragraph 5, SI). Pronounced solvent-dependent differences were found between the two complexes. In acetonitrile, **OsCOCl** exhibits the strongest emission (λ_{em} 550 nm), while **RuCOCl** is ~7-fold less emissive, as also witnessed by ϕ_L values of 15.6(6) × 10^{-3} and 2.24(9) × 10^{-3}, respectively (Table 1 and Table S1, SI). Water markedly affects the luminescence signals, with **OsCOCl** being almost completely quenched and **RuCOCl** retaining a residual signal. Interestingly enough, the *trans*-CO enriched **OsCOCl-67** is almost non-emissive compared to **OsCOCl** (Fig. 1a), hinting at a possible influence of the CO ligand geometry in the balance between radiative and non-radiative decay pathways.[28,29]

As a fundamental prerequisite for their PDT application, the singlet oxygen quantum yields (Φ_Δ) of the metal complexes were determined by direct measurement of the $^1O_2$ phosphorescence at 1270 nm upon irradiation of air-saturated acetonitrile solutions, a more reliable approach compared to the use of indirect probes, often sensitive to other ROS species.[30] Results for **OsCOCl** are reported in Fig. 1c, with those for the other compounds in paragraph 2 (SI); Φ_Δ values were determined as previously described[31,32] using $Ru(phen)_3Cl_2$ as a standard (Φ_Δ = 0.38 ± 0.06)[33] and are listed in Table 1. As shown, all complexes display strong sensitizing properties, with **OsCOCl** being almost 1.5-fold more efficient than **RuCOCl** (Φ_Δ = 0.88 ± 0.06 *vs.* Φ_Δ = 0.60 ± 0.06). The different ability to sensitize $^1O_2$ conferred by the two metals was further investigated by DFT and TDDFT calculations. Detailed information is reported in paragraph 5.2, SI. As shown in the Jablonski-like diagram of Fig. 1d, our results indicated significantly higher spin–orbit coupling (SOC) for **OsCOCl**, ~ 10 times higher relative to Ru(II), in line with the stronger spin–orbit coupling/heavy-atom effect of the former and therefore well corroborating the experimental findings.

Preliminary to the biological tests, the stability of the complexes in PBS solutions was assessed by UV-Vis spectroscopy. The absence of appreciable spectral variations in the dark over a total period of 24 hours demonstrated a remarkable stability under these conditions (Fig. S10, SI). Their photoreactivity was also evaluated spectrophotometrically in PBS and acetonitrile to monitor their structural integrity under prolonged LED irradiation (λ_{max} 462 nm, 160 mW, time up to 2 h). These experiments, complemented by HR ESI-MS analysis (Fig. S11 and S12, paragraph 4, SI), indicated a tendency, particularly pronounced for **RuCOCl**, for CO release/partial release upon extended photoactivation, also resulting in a detrimental effect on singlet oxygen sensitization. However, this effect remains negligible within the reduced irradiation duration of the PDT biological assays (*vide infra*). Yet, the investigation of these complexes as suitable photoCORMs represents an interesting aspect that will be explored in future studies. Focusing on the remarkable PDT potential of **RuCOCl** and **OsCOCl**, the biological behaviour of the complexes was preliminarily evaluated in A431 vulvar carcinoma cells, chosen as a human cancer model. The internalization of the complexes was first evaluated by confocal laser scanning fluorescence microscopy (CLSM), quantified by inductively coupled plasma mass spectrometry (ICP-MS) and then followed by evaluation of their photodynamic effect by MTT analysis (see SI for the experimental details). As shown by CLSM imaging (Fig. 2a), both **RuCOCl** and **OsCOCl** were promptly and efficiently internalized in tumoral cells, showing a marked time- and concentration-dependent uptake (1 to 3 h, 1–10 μM).

Table 1 Absorption and fluorescence maxima ($\lambda_{max}/\lambda_{em}$) of the complexes in CH_3CN and water, luminescence and $^1O_2$ quantum yields (ϕ_L and ϕ_Δ) in aerated acetonitrile

Complex	λ_{max}/nm (ε × 10^3/M^{-1} cm^{-1}) in CH_3CN	λ_{max}/nm (ε × 10^3/M^{-1} cm^{-1}) in H_2O	λ_{em}/nm in CH_3CN	λ_{em}/nm in H_2O	Φ_L CH_3CN (× 10^{-3})	Φ_L H_2O (× 10^{-3})	Φ_Δ $^1O_2$ CH_3CN
RuCOCl	260 (52.6), 312 (53.5), 396 (8.09), 408 (8.06)	262 (45.6), 312 (45.0), 396 (6.64), 408 (5.82)	571	614	2.24 ± 0.09	4.3 ± 0.2	0.60 ± 0.06
OsCOCl	240 (36.1), 262 (37.1), 321 (55.6), 395 (9.15), 412 (8.94)	265 (31.8), 321 (36.4), 395 (11.5), 412 (10.5)	550	—	15.6 ± 0.6	0.87 ± 0.06	0.88 ± 0.06

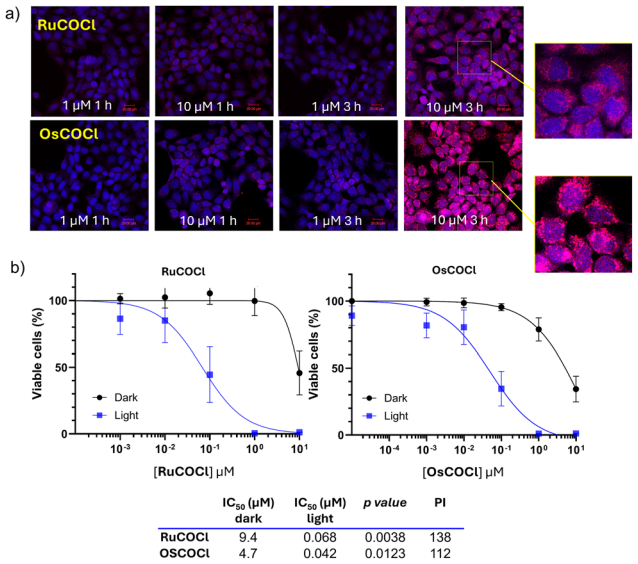

	IC_{50} (μM) dark	IC_{50} (μM) light	*p value*	PI
RuCOCl	9.4	0.068	0.0038	138
OSCOCl	4.7	0.042	0.0123	112

Fig. 2 (a) Time and dose-dependent cellular uptake of **RuCOCl** and **OsCOCl** (1–10 μM) in A431 cells by CLSM. DAPI was used to counterstain nuclei (λ_{exc} = 405 nm, λ_{em} = 461 nm), complex fluorescence appears in purple-red (λ_{exc} = 405 nm, λ_{em} = 600–640 nm). Confocal fluorescence images; scale bar = 20 μm. Magnified insets are provided for the 10 μM, 3 h incubation conditions for both **RuCOCl** and **OsCOCl**. (b) Cell viability by MTT assay in the dark or upon photoactivation (λ_{max} 462 nm, 160 mW): absorbance was normalized to untreated controls; dose–response curves were fitted by nonlinear regression and IC_{50} values compared using the extra sum-of-squares *F* test (n = 3).

ICP-MS quantification confirmed intracellular metal contents of approximately 200 ng of Ru and 450 ng of Os per 10^6 cells after 3 h incubation at 10 μM (Fig. S14, SI). Notably, both complexes tended to accumulate within the cytoplasmic region surrounding the DAPI-stained nuclei. In the dark, MTT assays (Fig. 2b) showed that **RuCOCl** was essentially non-toxic up to 1 μM, whereas **OsCOCl** caused a moderate decrease in cell viability of 20% at the same concentration. Upon 15 min photoactivation (λ_{max} = 462 nm, 160 mW), both compounds exhibited pronounced cytotoxic activity, consistent with their strong photosensitizing properties, resulting in a marked shift of the IC_{50} values from the micromolar to the sub-micromolar range (Fig. 2b). Interestingly, despite **OsCOCl**'s superior photophysical properties, **RuCOCl** exhibited the highest photoreactivity index (PI = 138), while the lower PI value of OsCOCl (*ca.* 112) likely reflects its higher dark cytotoxicity.

In summary, the aim of this comparative study is to highlight the potential of the two novel carbonylchlorido complexes **RuCOCl** and **OsCOCl** for PDT, beyond shedding light on the role of the metal in shaping their properties as effective photosensitizers. Following the synthesis, accomplished by introducing a central chemically controlled decarbonylation of the dicarbonylic precursors, our data evidenced the favourable features of **RuCOCl** and **OsCOCl** for their PDT application, in particular those inferred by Os(II), namely red-shifted absorption profiles and augmented emissive and sensitization properties compared to its lighter congener. DFT and TDDFT calculations were also undertaken to corroborate the experimental findings. Lastly, preliminary *in vivo* investigations confirmed the perspectives of these systems in the PDT of vulvar carcinoma, although the higher in the dark cytotoxicity of **OsCOCl** partially counteracts its superior photophysical properties.

Which metal therefore performs better? Clearly, there is no simple answer; the choice of metal has to be rather considered alongside the overall complex/drug design, taking into account the careful balance between reactivity, photophysical and biological properties of this largely underestimated class of potential PDT agents.

Conflicts of interest

The authors declare no conflicts of interest.

Data availability

The data supporting this article have been included as part of the supplementary information (SI). Supplementary information: detailed experimental procedures, additional tables and figures. See DOI: https://doi.org/10.1039/d5cc06225j.

Acknowledgements

G. E. G. and V. C. respectively thank Fondazione Umberto Veronesi and the Next Generation EU Project B12B23000300006, for the financial support.

References

1 J. Karges, *Angew. Chem., Int. Ed.*, 2022, **61**, e202112236.
2 L. Conti, E. Macedi, C. Giorgi, B. Valtancoli and V. Fusi, *Coord. Chem. Rev.*, 2022, **469**, 214656.
3 X. Y. Ng, K. W. Fong, L. V. Kiew, P. Y. Chung, Y. K. Liew, N. Delsuc, M. Zulkefeli and M. L. Low, *J. Inorg. Biochem.*, 2024, **250**, 112425.
4 Y. Xu, C. Li, S. Lu, Z. Wang, S. Liu, X. Yu, X. Li and Y. Sun, *Nat. Commun.*, 2022, **13**, 2009.
5 M. Li, J. Xiong, Y. Zhang, L. Yu, L. Yue, C. Yoon, Y. Kim, Y. Zhou, X. Chen, Y. Xu, X. Peng and J. S. Kim, *Chem. Soc. Rev.*, 2025, **54**, 7025.
6 Y.-A. Deng, S.-J. Tang, M.-F. Wang, X. Ren, X.-L. Li, L.-Z. Zeng, D.-N. Ren, M.-R. Wang, W.-L. Xiao, Z.-Y. Cai, D. Zhang, H. Zhang and F. Gao, *Inorg. Chem. Front.*, 2023, **10**, 4552–4561.
7 L. Conti, G. E. Giacomazzo, B. Valtancoli, M. Perfetti, A. Privitera, C. Giorgi, P. S. Sfragano, I. Palchetti, S. Pecchioli, P. Bruni and F. Cencetti, *Int. J. Mol. Sci.*, 2022, **23**, 13302.
8 K. M. Kuznetsov, K. Cariou and G. Gasser, *Chem. Sci.*, 2024, **15**, 17760–17780.
9 S. M. Meier-Menches, C. Gerner, W. Berger, C. G. Hartinger and B. K. Keppler, *Chem. Soc. Rev.*, 2018, **47**, 909–928.
10 A. Mani, T. Feng, A. Gandioso, R. Vinck, A. Notaro, L. Gourdon, P. Burckel, B. Saubaméa, O. Blacque, K. Cariou, J.-E. Belgaied, H. Chao and G. Gasser, *Angew. Chem., Int. Ed.*, 2023, **135**, e202218347.
11 M. Stitch, R. Z. Boota, A. S. Chalkley, T. D. Keene, J. C. Simpson, P. A. Scattergood, P. I. P. Elliott and S. J. Quinn, *Inorg. Chem.*, 2022, **61**, 14947–14961.
12 B. Carlson, G. D. Phelan, W. Kaminsky, L. Dalton, X. Jiang, S. Liu and A. K. Y. Jen, *J. Am. Chem. Soc.*, 2002, **124**, 14162–14172.
13 A. Gul, M. Ahmad, A. Ali, D. Boateng, L. Yang, Y. Kang and W. Liao, *Colloids Surf., B*, 2025, **255**, 114935.
14 H. Ishida, K. Fujiki, T. Ohba, K. Ohkubo, K. Tanaka, T. Terada and T. Tanaka, *J. Chem. Soc., Dalton Trans.*, 1990, 2155–2160.
15 J.-M. Lehn and R. Ziessel, *J. Organomet. Chem.*, 1990, **382**, 157–173.
16 M. N. Collomb-Dunand-Sauthier, A. Deronzier and R. Ziessel, *J. Phys. Chem.*, 1993, **97**, 5973–5979.

17 H. Ishida, H. Tanaka, K. Tanaka and T. Tanaka, *J. Chem. Soc., Chem. Commun.*, 1987, 131–132.
18 K. Tanaka, M. Morimoto and T. Tanaka, *Chem. Lett.*, 1983, 901–904.
19 S. P. Foxon, C. Metcalfe, H. Adams, M. Webb and J. A. Thomas, *Inorg. Chem.*, 2007, **46**(2), 409–416.
20 G. E. Giacomazzo, M. Schlich, L. Casula, L. Galantini, A. Del Giudice, G. Pietraperzia, C. Sinico, F. Cencetti, S. Pecchioli, B. Valtancoli, L. Conti, S. Murgia and C. Giorgi, *Inorg. Chem. Front.*, 2023, **10**, 3025–3036.
21 G. E. Giacomazzo, G. Mulas, I. Palchetti, L. Conti, F. Tadini-Buoninsegni, B. Valtancoli, F. Cencetti and C. Giorgi, *Bioinorg. Chem. Appl.*, 2025, 8899727.
22 L. Spiccia, G. B. Deacon and C. M. Kepert, *Coord. Chem. Rev.*, 2004, **248**, 1329–1341.
23 B. P. Sullivan, J. V. Caspar, T. J. Meyer and S. Johnson, *Organometallics*, 1984, **3**, 1241–1251.
24 E. Z. Jandrasics and F. R. Keene, *J. Chem. Soc., Dalton Trans.*, 1997, 153–160.
25 C. M. Kepert, G. B. Deacon, N. Sahely, L. Spiccia, G. D. Fallon, B. W. Skelton and A. H. White, *Inorg. Chem.*, 2004, **43**, 2818–2827.
26 E. C. Glazer, *Photochem. Photobiol.*, 2017, **93**, 1326–1328.
27 A. Hernández-García, L. Marková, M. D. Santana, J. Prachařová, D. Bautista, H. Kostrhunová, V. Novohradský, V. Brabec, J. Ruiz and J. Kašpárková, *Inorg. Chem.*, 2023, **62**, 6474–6487.
28 C. Daniel and A. Veillard, *Inorg. Chem.*, 1989, **28**, 1170–1173.
29 S. J. Carrington, I. Chakraborty, J. R. Alvarado and P. K. Mascharak, *Inorg. Chim. Acta*, 2013, **407**, 121–125.
30 S. Mondal, R. B. Jethwa, B. Pant, R. Hauschild and S. A. Freunberger, *Faraday Discuss.*, 2024, **248**, 175–189.
31 G. E. Giacomazzo, S. Doria, A. Revilla-Cuesta, N. De Monte, M. Pagliai, G. Pietraperzia, B. Valtancoli, T. Torroba, L. Conti, M. Di Donato and C. Giorgi, *Inorg. Chem.*, 2024, **63**, 6248–6259.
32 G. Sambucari, C. Coutant, A. Di Michele, G. E. Giacomazzo, P. Nun, V. Sol, N. Renard, T. Ouk, V. Coeffard and M. D. Donato, *Adv. Opt. Mater.*, 2025, **13**, 1–11.
33 L. Conti, A. Bencini, C. Ferrante, C. Gellini, P. Paoli, M. Parri, G. Pietraperzia, B. Valtancoli and C. Giorgi, *Chem. – Eur. J.*, 2019, **25**, 10606–10615.